



Article

Structural Nanocomposite Fabrication from Self-Assembled Choline Chloride Modified Kaolinite into Poly(Methylmethacrylate)

Dipti Saha, Mithun Kumar Majumdar, Ajoy Kumar Das, A.M. Sarwaruddin Chowdhury and Md. Ashaduzzaman *

Department of Applied Chemistry and Chemical Engineering, Faculty of Engineering and Technology, University of Dhaka, Dhaka 1000, Bangladesh

* Correspondence: azaman01@du.ac.bd; Tel.: +880-168-077-3734

Received: 28 June 2019; Accepted: 6 August 2019; Published: 13 August 2019



Abstract: Composite materials produced from indigenous nanoscale particles and synthetic polymers have created demand in the field of nanoscience and technology. Layered silicates are potential candidates for reinforcing the properties of composites. Here, we report the fabrication of nanocomposites using poly(methylmethacrylate) (PMMA) as the matrix and the Bijoypur clay of Bangladesh known as kaolinite (200–250 nm) as the filler via solution casting. Kaolinite was first modified using choline chloride to prepare core-shell particles through a precipitation technique and was used for self-assembled nanocomposite films preparation. A series of nanocomposites films using 0, 1, 3, 5 and 10% (*w/w*) modified kaolinite was prepared. The neat PMMA and nanocomposite films were characterized by attenuated total reflection infra-red (ATR-IR) spectroscopy and X-ray diffraction (XRD) techniques. The mechanical properties, thermal stability, and morphology of the films were investigated using a universal testing machine (UTM), a thermal gravimetric analyzer (TGA), and a scanning electron microscope (SEM). The nanocomposite films exhibited better mechanical properties and thermal stability than neat PMMA film. Development of such structural nanocomposite materials using naturally occurring nanoscale particles would play a crucial role in the field of materials science for packaging applications and separation technology.

Keywords: nano-composites; kaolinite; PMMA; choline chloride; tensile strength; self-assembled

1. Introduction

Nanoscale indigenous layered material and polymer composites are of great interest to the researchers due to the environmental considerations [1–5]. Nanostructured layered silicates incorporate higher mechanical, thermal stability, and barrier properties in the composite materials at relatively low filler contents compared to those of conventional composites [6–10]. The available naturally occurring nanostructures are montmorillonite, clay, silica and calcium carbonate. Kaolinite is composed of white, soft, and highly refractory clay particles [11]. Hydrated kaolinite ($\text{Al}_2\text{O}_3 \cdot 2\text{SiO}_2 \cdot 2\text{H}_2\text{O}$) maintains aluminosilicate with a 1:1 layered structure consisting of an octahedral aluminum hydroxide sheet and a tetrahedral silica sheet [12].

Due to the inherent rigid characteristic of a layered structure, kaolinite is not susceptible to interactions with functional polymers. Chemically modified kaolinite incorporates interfacial properties which can promote the compatibility and dispersion of the particles into a polymer matrix. Treatment of particles with epoxy functional silane coupling agent has been extensively used to examine the properties of calcined kaolin (CK_{ao}), TiO_2 in polyethylene terephthalate (PET) composites [13–16]. Polymer/clay nanocomposites is an interesting and very promising research area due to cost effectiveness, their high specific surface area, and their ease of availability from natural resources [17–19].

Recently work has been focused on developing polymer/clay nanocomposites using various polymers, such as polypropylene (PP), polyamide, polyimide, nylon, polystyrene (PS), ethylene vinyl acetate copolymer, polyethylene terephthalate, polyurethane, low density polyethylene (LDPE), high density polyethylene (HDPE), epoxy, PS/HDPE, PP/HDPE, and PP/LDPE [20–25]. A number of clay types have been used, including kaolinite, Illite, Bentonite, Chlorite, and Montmorillonite [26,27]. On the other hand, considering the outstanding mechanical properties, thermal capability and electric performance, poly(methylmethacrylate) (PMMA) has been widely used as the matrix. Many potential applications [28] of PMMA have evoked intense interest in PMMA based composites. As a result, many composites of PMMA-clay have been prepared by suspension polymerization, emulsion polymerization, and bulk polymerization, etc. [29–31]. But PMMA–choline chloride modified kaolinite composites are rare.

In the last few years, researchers have begun to fabricate PMMA based composites. In 2015, Kumar, et al. [32] reported nanocomposites consisting of poly(methyl methacrylate) (PMMA)/clay with different compatibilizers (PP-g-MA, PE-g-MA and PS-g-MA), with 5 wt % nanoclay. Poly(methyl methacrylate) (PMMA) and montmorillonite (MMT), modified with 15–35 wt % octadecylamine and 0.5–5 wt % aminopropyltriethoxysilane, and different compatibilizers, such as polypropylene-grafted maleic anhydride (PP-g-MA), polyethylene-grafted maleic anhydride (PE-g-MA), and polystyrene-block-poly(ethyleneterephthalate)-block-polystyrene-graft-maleic anhydride (PS-g-MA) were used. In 2014, Nabirqudri, et al. [33] developed composites films using poly(methyl methacrylate) and cocoamphodipropionate modified montmorillonite. In 2006, Hani, et al. [34] reported nanocomposites of dehydrogenated tallow quaternary ammonium modified montmorillonite clay and poly(methylmethacrylate), and also described the affect of nanoclay on mechanical properties. Besides, in 2012, Modak, et al. [35] reported a well-dispersed poly(methylmethacrylate) (PMMA)–bentonite clay composite by emulsion polymerization using methyl methacrylate (MMA) monomer and 3% sodium carbonate treated bentonite clay.

Hydrophilic kaolinite surface is thermodynamically incompatible with most hydrophobic and thermoplastic polymers of commercial importance, such as poly(methylmethacrylate) (PMMA), polypropylene [36], and polyethylene [37]. For favorable thermodynamic interactions at the molecular level of a specific polymer with kaolinite, organic modification of the kaolinite is required. Therefore, for the first time, we have used choline chloride as the modifying agent to prepare a new composite material. Choline chloride contains amino (–NH₂) and hydroxyl (–OH) functional groups, which can serve as coordination and reaction sites, and as a result it is used as an adsorbent. Negatively charged kaolinite is electrostatically interacted with by protonated amine groups (–NH₃) of choline chloride to form a choline chloride modified kaolinite. In this article, we have fabricated PMMA/choline chloride modified, kaolinite nanocomposite, self-assembled films by solution casting. This film would show improved mechanical properties and thermal stability, and can be used for advanced applications in the field of frontier science and technology.

2. Materials and Methods

2.1. Materials

Kaolinite was collected from Bijoypur (Netrokona, Bangladesh). It was white crystalline powder. Poly(methylmethacrylate), (PMMA) (Mw 1,20,000) was procured from Sigma-Aldrich (Stockholm, Sweden). Choline chloride solution (40% w/w) was procured from Puyer (Nantong) BioPharma Co., LTD., Nantong, China. NaOH was supplied by Active Fine Chemicals Limited, Dhaka, Bangladesh. Ethanol and chloroform (CH₃Cl) were purchased from Merck KGaA, 64271 Darmstadt, Germany.

2.2. Methods

2.2.1. Fabrication of Poly(methylmethacrylate)/Choline Chloride Modified Kaolinite PMMA/CCMK Nanocomposite Films

Five films with different weight ratios of choline chloride modified kaolinite (CCMK) and poly (methylmethacrylate) (PMMA) were prepared as shown in Table 1. At first, 3 mL solution of PMMA in chloroform (CH_3Cl) was taken in each five different small glass vials. Then after leaving one vial (without addition of CCMK), 10, 30, 50 and 100 mg of CCMK were charged into the vials containing PMMA solution and stirred for 5 min. The resulting suspensions were sonicated with the help of a microprocess controlled bench-top ultrasound cleaner (sonicator) for 5 min and the sonicated mixtures were allowed to stir for 5 min again to make a homogenous suspension. The clear suspensions were then cast onto five glass frames (length and width of the glass plates were 7.62 cm and 2.54 cm respectively) and then the suspensions were turned into films via atmospheric drying for 48 h as shown in Figures S1 and S2 in the supplementary materials. The dried films were then pulled out from the glass frame and cut into desired pieces for different purposes of use. Each of the sample films were subjected to analysis, and twice fabricated from the three batches of each composition.

Table 1. Compositional variation of nanocomposite films produced from poly(methylmethacrylate) (PMMA) and chloride modified kaolinite (CCMK).

Composite Identity	PMMA % (w/w)	CCMK % (w/w)	PMMA:CCMK
CK ₀ PNC	100	0	100:0
CK ₁ PNC	99	1	99:01
CK ₃ PNC	97	3	97:03
CK ₅ PNC	95	5	95:05
CK ₁₀ PNC	90	10	90:10

2.2.2. Characterizations

(1) Attenuated total reflectance infrared (ATR-IR) spectrophotometer

ATR-IR spectra of samples were recorded on a FT-IR Shimadzu IR Prestige 21 (Shimadzu, Corporation, Kyoto, Japan) in the wave number range of 4000–400 cm^{-1} ; resolution: 4 cm^{-1} ; scan number 30.

(2) X-ray diffractometer (XRD)

The samples were examined by an x-ray diffractometer (Ultima IV, Rigaku Corporation, Tokyo, Japan) at room temperature. At first, the samples were ground into fine powders using a mortar and pestle. Cu K α radiation ($\lambda = 0.154 \text{ nm}$), from a broad focused Cu tube operated at 40 KV and 40 mA, was applied to the samples for measurement. The XRD patterns of the samples were measured in the continuous scanning mode with a scan speed 5°/min and in the scan range of 10 to 60°. Bragg's law was used to compute the basal spacing of the crystalline samples.

(3) Thermogravimetric analyzer (TGA)

The thermogravimetric analyses of the samples were recorded on a thermogravimetric analyzer TGA-50H (Shimadzu, Kyoto, Japan). The samples were heated from room temperature to 700 °C under a nitrogen atmosphere at the flow rate of 19 mL/min and at the heating rate of 10 °C/min using an alumina cell. The weight of the samples was taken to be 10 mg for the experiment. Total hold time at 700 °C was 5 min.

(4) Universal testing machine (UTM)

The mechanical properties, tensile strength (TS), and elongation at break (Eb) of the nanocomposite films were examined with a universal strength tester machine (Titan, model 1410-Titan⁵, Shanghai,

China). The film length and width used were 50 mm and 20 mm, respectively. Dry films with an average thickness of around 150 μm were obtained by measuring with a Phynix digital micrometer. All the test samples were conditioned at 20 °C and 50% relative humidity. All the tests were carried out under the same conditions. The following equations were used to measure the tensile properties.

$$\text{Tensile strength, TS (MPa)} = \frac{\text{Load}}{\text{Thickness} \times \text{Width}} \quad \text{and} \quad \text{Elongation at break, Eb (\%)} = \frac{\text{Displacement}}{\text{Gauze Length}}$$

(5) Scanning electron microscope (SEM)

The morphology of the samples was analyzed by an analytical scanning electron microscope (JEOL JSM-6490LA, Tokyo, Japan) operated at an accelerating voltage of 20 KV. In order to get further insight into the morphology, microstructures of the samples were examined at the 5 μm scale with 500 magnifications without coating, and using an only partial vacuum.

3. Results and Discussion

3.1. ATR-IR Spectral Analysis

A comparison of the ATR-IR spectrum of nanocomposites produced using 1, 3, 5, and 10% (*w/w*) modified choline chloride kaolinite, self-assembled in PMMA and neat PMMA is shown in Figure 1. (In the supplementary materials, Figure S3 represents the ATR-IR spectra of kaolinite, choline chloride modified kaolinite nanocomposites, and choline chloride.) The band around 3690 cm^{-1} assigned for kaolinite was absent in the nanocomposite film fabricated using 1% *w/w* CCMK (curve D in Figure 1), but the peak gradually appeared as the kaolinite content increased, as shown in the curves A–C in Figure 1. The absorption band at 1730.15 cm^{-1} is the characteristic peak at PMMA polymer which denotes the $>\text{C}=\text{O}$ group present in the PMMA polymer (curve E in Figure 1). The band at 943.19 cm^{-1} is the $-\text{C}-\text{H}$ bending vibration together with the bands at 1028.06 cm^{-1} and 852.54 cm^{-1} in the acrylate group in PMMA [32]. The band at 1452.40 cm^{-1} can be attributed to the bending vibration of the $\text{C}-\text{H}$ bonds of the $-\text{CH}_3$ group. The two bands at 2931.80 cm^{-1} and 2872.01 cm^{-1} were assigned to the $\text{C}-\text{H}$ bond stretching vibrations of the $-\text{CH}_3$ and $-\text{CH}_2-$ groups, respectively. Furthermore, there was another weak absorption band at 3446.79 cm^{-1} which was attributed to the $-\text{OH}$ group stretching of physisorbed moisture [38]. The absorption bands at 1107.14 cm^{-1} , 1161.15 cm^{-1} , and 1247.87 cm^{-1} were attributed to the $\text{C}-\text{O}-\text{C}$ stretching vibration. The two bands at 1381.03 cm^{-1} and 763.81 cm^{-1} were attributed to the methyl group vibrations. The characteristic absorption band at 1730.15 cm^{-1} represents stretching vibration of $\text{C}=\text{O}$ of pure PMMA. In all composite films, the stretching vibration of carbonyl group ($\text{C}=\text{O}$) group appearing at the frequency of 1730.15 cm^{-1} for pure PMMA moves to lower positions at 1720 cm^{-1} . Furthermore, the absorption peak at 3446.79 cm^{-1} assigned for OH stretching in PMMA was also shifted to 3393 cm^{-1} . In addition, the absorption band at 1166 cm^{-1} for the $\text{C}-\text{O}-\text{C}$ stretching vibration of PMMA was shifted to 1150–1161 cm^{-1} in nanocomposites films. That result proves that there was an interaction between CCMK and PMMA molecular chains [39].

3.2. XRD Analysis

In the Figure 2A the broad peak at the position (2θ) with *d*-spacing was found for the crystalline segment of PMMA in neat film which was almost unchanged in the nanocomposite films of CK₁₀PNC. Furthermore, the sharp peaks in the nanocomposite films indicate the presence of kaolinite, and these peaks were in the similar positions of pure kaolinite. The non-variable and non-shifting of peak position clearly indicates that the nanocomposites consisted of un-intercalated nor adhered kaolinite, due to the electrostatic interaction. The XRD pattern of pure kaolinite has been presented in the supplementary materials in Figure S4.

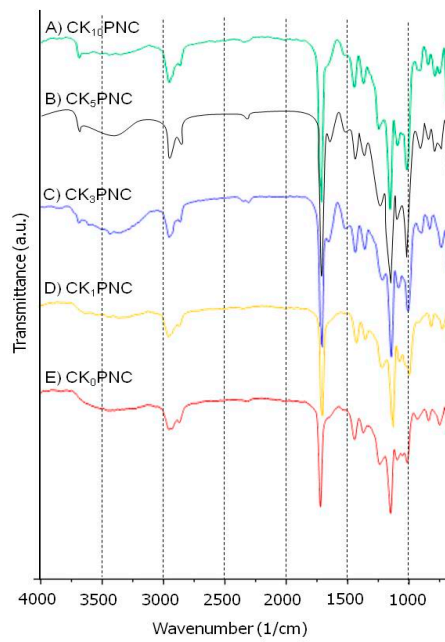


Figure 1. Attenuated total reflection infra-red (ATR-IR) spectra of films produced from nanocomposite of poly(methylmethacrylate) (PMMA) and choline chloride modified kaolinite (CCMK). (A) CK₁₀PNC, (B) CK₅PNC, (C) CK₃PNC, (D) CK₁PNC and neat PMMA (E) CK₀PNC.

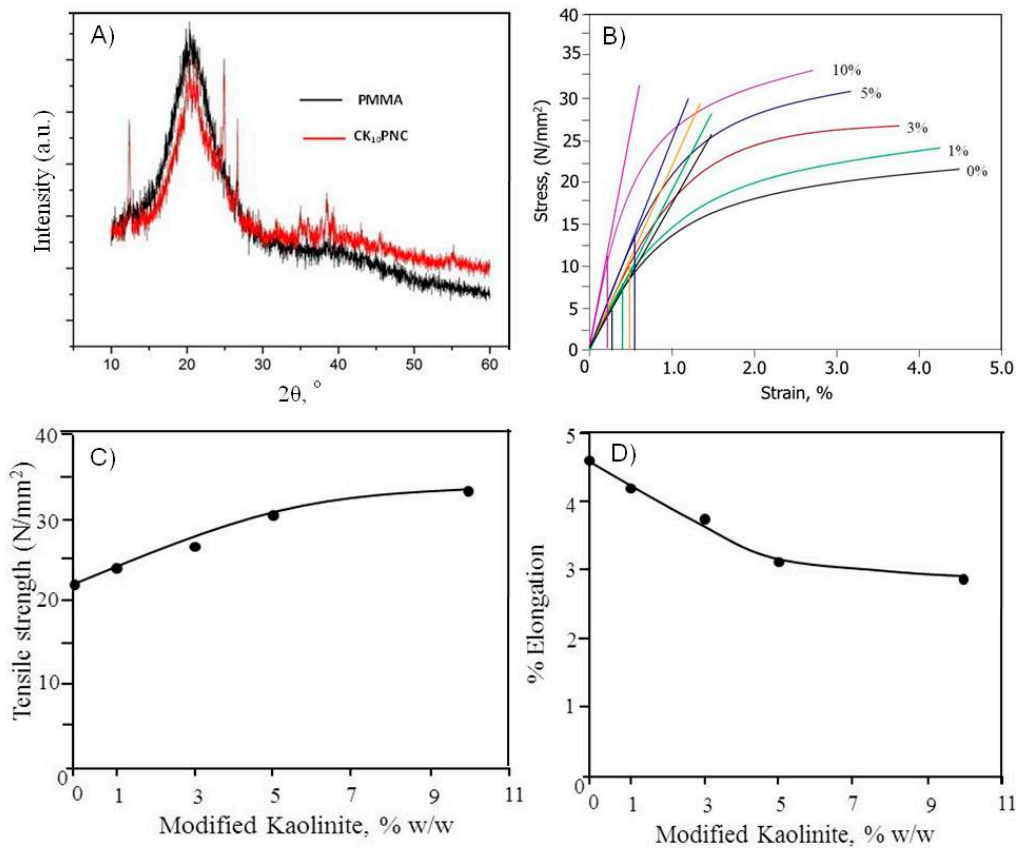


Figure 2. XRD patterns of CK₀PNC, CK₁₀PNC. (A) Stress versus strain (%) curve. (B) The effect of modified kaolinite on the tensile strength (N/mm²) of nanocomposite films. (C) The effect of CCMK on the elongation at break (%) of the PMMA/CCMK nanocomposite films (D).

3.3. Studies of Mechanical Properties of Nanocomposite Films

Films fabricated from neat PMMA and choline chloride modified kaolinite composites were subjected to various kinds of stress in order to study the mechanical properties for determining the performance of the structural materials [40,41]. With the view of these objectives, strain-stress relationships of the fabricated films has been investigated, first with the Figure 2B, later with the tensile strength and elongation at break of films plotted as a function of the choline chloride modified kaolinite contents and CK₅PNC, as shown in Figure 2C,D for deep discussion.

3.3.1. Stress–Strain Relationship

Figure 2B shows the engineering stress–strain relationship curve (tensile) for self-assembled nanocomposite films with different quantities of CCMK. The tensile property of a material is shown by its stress–strain curve. Strain at yield was found to increase linearly with applied stress. It reaches maximum and then falls down. The curves have two regions—one is elastic region and another is plastic region. From the Figure 2B, it was found that composites deform elastically and then plastic deformation starts. The vertical lines parallel to the y-axis from the strain at yield point separate elastic and plastic zones of corresponding engineering stress versus strain curve; the area in the left zone is called elastic zone, where the reversible deformation occurs, and the right zone is where the permanent deformation occurs up to the break or failure.

The film produced from neat PMMA (0%) shows the minimum elasticity and maximal plastic behavior; it indicates that the reversible deformation occurs within a very short range of 0.25% strain at yield. As the addition of modified kaolinite increased from 0 to 10% *w/w*, the strain at yield was first increased from 0.25 to 0.60% for CK₅PNC films, and then decreased to 0.20% for CK₁₀PNC (also shown in supplementary materials, Figure S5). It means that the matrix PMMA was sufficient to cover the CCMK particles and to form a kaolinite cored, PMMA-thick, shell-based homogeneously dispersed film produced from CK₅PNC. But in case of CK₁₀PNC film, the PMMA matrix was not sufficient to cover in that manner, as was the case for the CK₁PNC to CK₅PNC films formed. Therefore, the particles were agglomerated, and the soft insufficient polymeric phase became hard and brittle. As a result, CK₅PNC film shows higher tensile strength (stress) than that of CK₁₀PNC film.

3.3.2. Tensile Strength Measurement

The tensile strength of the fabricated films was measured and plotted against the modified kaolinite content, as shown in the Figure 2C. It is observed that the tensile strength of the nanocomposite was increased with the increase of choline chloride modified kaolinite content, up to 5% *w/w*, and then it was slowed down. The tensile strength of the neat PMMA film CMKNC was 22 N/mm². However, for CMK₅NC film, the tensile strength was 31 N/mm² and for CMK₁₀NC film, the tensile strength was 33 N/mm². It is clear that the rate of increment of tensile strength up to 5% was higher than the rate within the range of 5 to 10% modified kaolinite.

3.3.3. Elongation at Break

The influence of choline chloride modified kaolinite in nanocomposites films on the elongation at break is shown in Figure 2D. It is evident that elongation at break rapidly declined with the increase of CCMK down to 5% by weight but very slowly decreased after 5% CCMK content in nanocomposites films. The elongation of break of neat PMMA film (CK₀PNC) was about 4.6%. However, at 5% CCMK containing film (CK₅PNC), the elongation at break of the film was decreased drastically to 2.9%.

Figure 3 shows the schematic illustration, starting from the left with neat PMMA film, denoted as CK₀PNC, possess polymeric crystalline phase only. In the absence of CCMK (fillers), polymer film becomes very soft. With the addition of CCMK, the crystalline phase was increased in the nanocomposite film. Therefore, due to the choline chloride shell of CCMK, the PMMA matrix attached strongly with the interface and controlled the thickness of the layer (steyn or boundary layer) around

the CCMK, as evident on the right of Figure 3. Since sufficient PMMA matrix remained in the CK₁PNC film, the elastic and plastic behavior did not change remarkably when compared to neat PMMA (CK₀PNC) film. The film CK₅PNC contained 5% CCMK; the whole PMMA matrix was used to cover the interface equally, and self-assembled stable CCMK incorporated better mechanical properties.

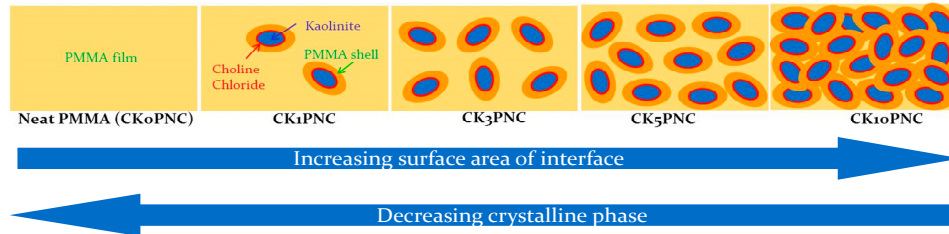


Figure 3. Schematic illustrations of neat PMMA film and the composite films to show the impact on interface and crystallinity of modified kaolinite.

3.4. Thermo Gravimetric Analysis (TGA)

The TGA thermogram of neat PMMA showed the weight loss profile at various temperatures, as shown in Figure 4. The first weight loss step was seen in the temperature range of 22–100 °C, corresponding to the weight loss of moisture (around 6%). Under nitrogen flow, a non-oxidative thermal degradation occurs in pure PMMA, which was observed in the temperature range of 280–430 °C, indicating the de-propagation to the end of PMMA chain, first order termination of the PMMA chain, vaporization, and elimination of volatile products [42]. The degradation of PMMA is accelerated above 280 °C owing to the formation of crosslinked and cyclic structures. However, the PMMA degradation appears to proceed by side-group depolymerization and random-chain scission depolymerization along with the diffusion of gas-phase nitrogen [43]. It degrades to tertiary alkyl free radical or secondary alkyl free radical, and the methyl methacrylate monomer or tertiary free radical. A char formation occurs after 400 °C, and was decomposed at about 450 °C leaving residue of about 1.6% *w/w* at the final temperature 700 °C.

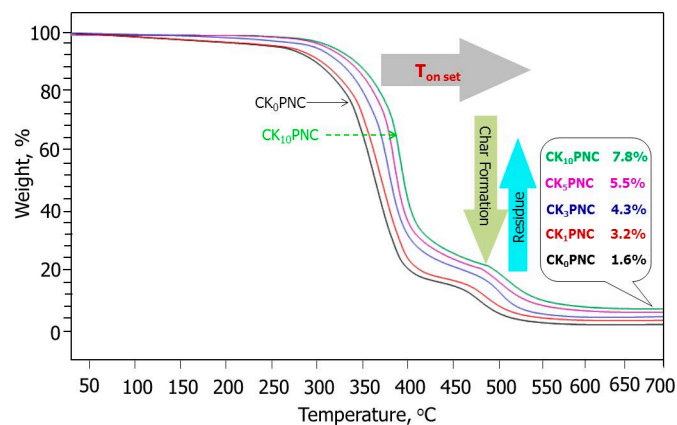


Figure 4. Thermograms of neat PMMA film and nanocomposite films.

The thermal degradation of nanocomposites films fabricated using 1, 3, 5, and 10% (*w/w*) CCMK, denoted as CK₁PNC, CK₃PNC, CK₅PNC and CK₁₀PNC films, showed almost similar patterns of weight loss, with higher thermal stabilities, as shown in Table 2. There was a progressive increase of the thermal stability of nanocomposites with the increase of CCMK amount in the nanocomposite films. The neat PMMA film was least thermally stable and CK₁₀PNC was the most thermally stable. As the CCMK content increased, the nanocomposites film exhibited a significant delay in weight loss at temperatures greater than 300 °C. The temperature at 50% weight loss increased from 370 °C to

385 °C, with an increase in CCMK content from 0 to 10%. Interestingly, after decomposition, the nanocomposites films yielded charred residue proportional to their CCMK content. The yield of polymeric charred residue along with bone dried kaolinite at 700 °C increased from 1.6% to 3.2%, 4.3%, 5.5% and 7.8% *w/w* with an increase in CCMK content from 0% to 1%, 3%, 5% and 10% *w/w* respectively.

Table 2. Thermogravimetric profile of pure PMMA and composite films recorded from thermographs.

Composites	Decomposition Starts at °C	Char Formation at °C	Decomposition Ends at °C	Residue% (<i>w/w</i>), at 700 °C
CK ₀ PNC	280	450	562	1.6
CK ₁ PNC	288	460	565	3.2
CK ₃ PNC	300	470	570	4.3
CK ₅ PNC	312	482	585	5.5
CK ₁₀ PNC	315	487	590	7.8

3.5. Scanning Electron Microscope (SEM) Morphological Studies of Nanocomposites Films

SEM micrographs have been used to investigate the morphologies of kaolinite, virgin PMMA film and the films fabricated from self-assembled modified kaolinite into PMMA matrix. Images of the morphology of pure kaolinite and choline chloride modified kaolinite are available in the supplementary materials in Figure S6.

Fabrication of PMMA/CCMK nanocomposites brought significant variation in the morphologies. The nanocomposites revealed uniform and smooth appearances with small irregularities and smaller or larger bumps with varying degrees of roughness.

Figure 5A–E shows SEM images of the pure PMMA films and the nanocomposite films produced from 1, 3, 5, and 10% *w/w* modified kaolinite and PMMA matrix. It is obvious that the pure PMMA film surface is very smooth. The composite film CK₁PNC showed that few particles are scattered within the film but CK₃PNC film appeared to be along with some bulk structure; that could be due to the entropic effect and the change of dielectric constant of the medium. The variation of the dispersion medium (PMMA) and dispersed phase (CCMK) creates a new environment within the composite in terms of energy distribution within the particles which dominate the self-assembly phenomena. Furthermore, increased modified kaolinite in CK₅PNC films leads to their homogeneous dispersion within the matrix, because an adequate interaction occurs between solid CCMK and PMMA phases, due to the uniform mixing of the system. An agglomeration of modified kaolinite particles in CK₁₀PNC film which was suffering from lack of matrix came out of the film surface with sharp edges.

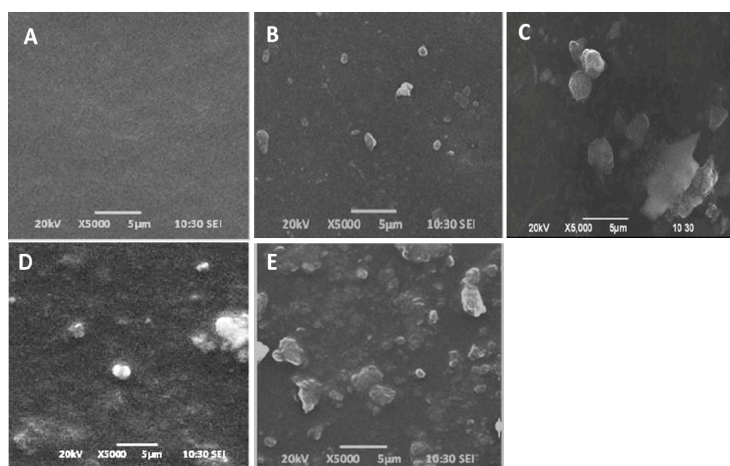


Figure 5. SEM images of virgin PMMA film (A) and the composites CK₁PNC (B), CK₃PNC (C), CK₅PNC (D), and CK₁₀PNC (E) films.

4. Conclusions

In the present study, self-assembled choline chloride modified kaolinite (CCMK) and polymethyl methacrylate (PMMA) nanocomposite films were fabricated by a simple casting method. Nanocomposites showed higher thermal stability, tensile strength and reduced elongation percentages at breaking points compared to those of neat PMMA film. Among the films, CK₅PNC showed the best mechanical properties. The film of CK₅PNC showed an optimum tensile strength of 31 N/mm² and about 0.60% strain at yield, which indicates, the film exhibited maximum elasticity with remarkable load bearing capacity. Although CK₁₀PNC film showed the highest tensile strength (33 N/mm²), the film also exhibited the lowest strain (0.20%). The percentage of elongation at break of nanocomposite films decreased with the increase of CCMK. Furthermore, thermal stability of CK₅PNC film was found almost similar to that of CK₁₀PNC film. Scanning electron microscopy images of CK₅PNC film showed a homogeneously distributed kaolinite smooth surface. The nanocomposite films created from modified indigenously layered material and lipophilic synthetic polymer could play important role in the field of packaging industry, and would be economical if applied in nanoscience and nanotechnology.

Supplementary Materials: The following are available online at <http://www.mdpi.com/2504-477X/3/3/83/s1>: Figure S1: Schematic illustration of fabrication technique of nanocomposite films; Figure S2: Optical camera images of nanocomposite films before (a) and after drying (b); Figure S3: ATR-IR spectra of kaolinite (a), choline chloride modified kaolinite nanocomposites (b) and choline chloride (c); Figure S4: XRD patterns of kaolinite and choline chloride modified kaolinite; Figure S5: Engineering stress–strain relationships; Figure S6: SEM images of kaolinite (A) and choline chloride modified kaolinite (B) respectively.

Author Contributions: Conceptualization, M.A.; data curation, A.K.D. and A.M.S.C.; formal analysis, A.M.S.C.; investigation, D.S.; methodology, M.K.M.; software, M.K.M. and M.A.; supervision, M.A.; validation, A.K.D.; visualization, M.A.; writing—original draft, D.S.; writing—review and editing, M.A.

Funding: This research was funded by Bangladesh University Grants Commission for University Teacher research allocation, grant number: Reg/Admin-3/58735.

Acknowledgments: The authors are grateful to the Centre for Advanced Research in Sciences (CARS), University of Dhaka, Bangladesh for providing partial analytical support to carry out this research work.

Conflicts of Interest: The authors declare no conflict of interest.

References

1. Cavallaro, G.; Lazzara, G.; Massaro, M.; Milioto, S.; Noto, R.; Parisi, F.; Riela, S. Biocompatible poly(N-isopropylacrylamide)-halloysite nanotubes for thermoresponsive curcumin release. *J. Phys. Chem. C* **2015**, *119*, 8944–8951. [[CrossRef](#)]
2. Fakhrullina, G.I.; Akhatova, F.S.; Lvov, Y.M.; Fakhrullin, R.F. Toxicity of halloysite clay nanotubes In Vivo: A Caenorhabditis elegans study. *Environ. Sci.: Nano*. **2015**, *2*, 54–59. [[CrossRef](#)]
3. Cavallaro, G.; Lazzara, G.; Konnova, S.; Fakhrullin, R.; Lvov, Y. Composite films of natural clay nanotubes with cellulose and chitosan. *Green Mater.* **2014**, *2*, 232–242. [[CrossRef](#)]
4. Costache, M.C.; Heidecker, M.; Manias, E.; Wilkie, C.A. Preparation and characterization of poly (ethylene terephthalate)/clay nanocomposites by melt blending using thermally stable surfactants. *Polym. Adv. Technol.* **2006**, *17*, 764–771. [[CrossRef](#)]
5. Ghasemi, H.; Carreau, P.J.; Kamal, M.R.; Uribe-Calderon, J. Preparation and characterization of PET/clay nanocomposites by melt compounding. *Polym. Eng. Sci.* **2011**, *51*, 1178–1187. [[CrossRef](#)]
6. Gorrasi, G.; Pantani, R.; Murariu, M.; Dubois, P. PLA/Halloysite nanocomposite films: Water vapor barrier properties and specific key characteristics. *Macromol. Mater. Eng.* **2014**, *299*, 104–115. [[CrossRef](#)]
7. Pegoretti, A.; Kolarik, J.; Peroni, C.; Migliaresi, C. Recycled poly (ethylene terephthalate)/layered silicate nanocomposites: morphology and tensile mechanical properties. *Polymer* **2004**, *45*, 2751–2759. [[CrossRef](#)]
8. Wang, Y.; Gao, J.; Ma, Y.; Agarwal, U.S. Study on mechanical properties, thermal stability and crystallization behavior of PET/MMT nanocomposites. *Composites Part B* **2006**, *37*, 399–407. [[CrossRef](#)]
9. Ghasemi, H.; Carreau, P.J.; Kamal, M.R.; Tabatabaei, S.H. Properties of PET/clay nanocomposite films. *Polym. Eng. Sci.* **2012**, *52*, 420–430. [[CrossRef](#)]

10. Ghanbari, A.; Heuzey, M.C.; Carreau, P.J.; Ton-That, M.T. Morphology and properties of polymer/organoclay nanocomposites based on poly (ethylene terephthalate) and sulfopolyester blends. *Polym. Int.* **2013**, *62*, 439–448. [[CrossRef](#)]
11. Shnean, Z.Y. Effect of grain and calcinations kaolin additives on some mechanical and physical properties on low density polyethylene composites. *Al-Khwarizmi Eng. J.* **2008**, *4*, 37–44.
12. Bergaya, F.; Lagaly, G. *Hand Book of Clay Science*; Elsevier: Amsterdam, Netherlands, 2006; pp. 1–18.
13. Zhao, J.; Milanova, M.; Warmoeskerken, M.; Dutschk, V. Surface modification of TiO₂ nanoparticles with silane coupling agents. In *Colloids and Surfaces A: Physicochemical and Engineering Aspects*; Gradzielski, M., Miller, R., Starov, V., Eds.; Elsevier: Amsterdam, Netherlands, 2012; Volume 413, pp. 273–279.
14. Wen, B.; Xu, X.; Gao, X.; Ding, Y.; Wang, F.; Zhang, S.; Yang, M. Highly exfoliated poly (ethylene terephthalate)/clay nanocomposites via melt compounding: Effects of silane grafting. *J. Polym. Plast. Technol. Eng.* **2011**, *50*, 362–371. [[CrossRef](#)]
15. Spencer, M.W.; Hunter, D.; Knesek, B.; Paul, D.R. Morphology and properties of polypropylene nanocomposites based on a silanized organoclay. *Polymer* **2011**, *52*, 5369–5377. [[CrossRef](#)]
16. Kim, E.S.; Shim, J.H.; Woo, J.Y.; Yoo, K.S.; Yoon, J.S. Effect of the silane modification of clay on the tensile properties of nylon 6/clay nanocomposites. *J. Appl. Polym. Sci.* **2010**, *117*, 809–816. [[CrossRef](#)]
17. Lazzara, G.; Cavallaro, G.; Abhishek, P.; Fakhrullin, R.; Anna, S.; Vladimir, V.; Yuri, L. An assembly of organic–inorganic composites using halloysite clay nanotubes. *Curr. Opin. Colloid Interface Sci.* **2018**, *35*, 42–50. [[CrossRef](#)]
18. Mohan, T.P.; Kanny, K. Effects of synthetic and processing methods on dispersion characteristics of nanoclay in polypropylene polymer matrix composites. *Mater. Sci. Appl.* **2011**, *2*, 785–800. [[CrossRef](#)]
19. Cavallaro, G.; Danilushkina, A.A.; Evtugyn, V.G.; Lazzara, G.; Milioto, S.; Parisi, F.; Rozhina, E.V.; Fakhrullin, R.F. Halloysite nanotubes: Controlled access and release by smart gates. *Nanomaterials* **2017**, *7*, 199. [[CrossRef](#)]
20. Okada, A.; Kawasumi, M.; Usuki, A.; Kojima, Y.; Kurauchi, T.; Kamigaito, O. Synthesis and properties of Nylon-6/Clay hybrids. *Polym. Based Mol. Compos.* **1990**, *171*, 45–50.
21. Pegoretti, A.; Dorigato, A.; Penati, A. Tensile mechanical response of polyethylene-clay nanocomposites. *eXPRESS Polym. Lett.* **2007**, *1*, 123–131. [[CrossRef](#)]
22. Agubra, V.; Owuor, P.; Hosur, M. Influence of nanoclay dispersion methods on the mechanical behavior of E-glass/epoxy nanocomposites. *Nanomaterials* **2013**, *3*, 550–563. [[CrossRef](#)]
23. George, T.S.; Asha Krishnan, K.; Anjana, R.; George, K.E. Studies on nano kaolin clay reinforced PS-HDPE nanocomposites. *Indian J. Adv. Chem. Sci.* **2013**, *1*, 201–206.
24. Anjana, R.; George, K. Reinforcing effect of nano kaolin clay on PP/HDPE blends. *Int. J. Eng. Res. Ind. Appl.* **2012**, *2*, 868–872.
25. Mustafa, S.N. Effect of kaolin on the mechanical properties of polypropylene/polyethylene composite material. *Diyala J. Eng. Sci.* **2012**, *5*, 162–178.
26. Ghosh, A. Nano-clay particle as textile coating. *Int. J. Eng. Technol. IJET-IJENS* **2011**, *11*, 40–43.
27. Srinivasan, R. Advances in application of natural clay and its composites in removal of biological, organic, and inorganic contaminants from drinking water. *Adv. Mater. Sci. Eng.* **2011**, *2011*, 872531. [[CrossRef](#)]
28. El-Bashir, S.M.; AlSalhi, M.S.; Al-Faifi, F.; Alenazi, W.K. Spectral properties of PMMA films doped by perylene dyestuffs for photoselective greenhouse cladding applications. *Polymers* **2019**, *11*, 494. [[CrossRef](#)]
29. Huang, X.; Brittain, W.J. Synthesis and characterization of PMMA nanocomposites by suspension and emulsion polymerization. *Macromolecules* **2001**, *34*, 3255–3260. [[CrossRef](#)]
30. Su, S.; Wilkie, C.A. Exfoliated poly (methyl methacrylate) and polystyrene nanocomposites occur when the clay cation contains a vinyl monomer. *J. Polym. Sci. Part A: Polym. Chem.* **2003**, *41*, 1124–1135. [[CrossRef](#)]
31. Yeh, J.M.; Liou, S.J.; Lin, C.Y.; Cheng, C.Y.; Chang, Y.W.; Lee, K.R. Anticorrosively enhanced PMMA–clay nanocomposite materials with quaternary alkylphosphonium salt as an intercalating agent. *Chem. Mater.* **2002**, *14*, 154–161. [[CrossRef](#)]
32. Kumar, M.; Arun, S.; Upadhyaya, P.; Pugazhenthii, G. Properties of PMMA/clay nanocomposites prepared using various compatibilizers. *Int. J. Mech. Mater. Eng.* **2015**, *10*, 7. [[CrossRef](#)]
33. Nabirqudri, S.A.M.; Roy, A.S.; Prasad, M.A. Electrical and mechanical properties of free-standing PMMA–MMT clay composites. *J. Mater. Res.* **2014**, *29*, 2957–2964. [[CrossRef](#)]

34. Jo, C.; Fu, J.; Naguib, H.E. Constitutive modeling for intercalated PMMA/clay nanocomposite foams. *Polym. Eng. Sci.* **2006**, *46*, 1787–1796. [[CrossRef](#)]
35. Modak, S.K.; Mandal, A.; Chakrabarty, D. Studies on synthesis and characterization of poly (methyl methacrylate)-bentonite clay composite by emulsion polymerization and simultaneous in situ clay incorporation. *Polym. Compos.* **2013**, *34*, 32–40. [[CrossRef](#)]
36. Mittal, V. Polymer layered silicate nanocomposites: a review. *Materials* **2009**, *2*, 992–1057. [[CrossRef](#)]
37. Katz, H.S.; Milewki, J.V. *Handbook of Fillers and Reinforcements for Plastics*; Van Nostrand Reinhold: New York, NY, USA, 1978.
38. Duan, G.; Zhang, C.; Li, A.; Yang, X.; Lu, L.; Wang, X. Preparation and characterization of mesoporous zirconia made by using a poly (methyl methacrylate) template. *Nanoscale Res. Lett.* **2008**, *3*, 118–122. [[CrossRef](#)]
39. Youssef, A.M.; Malhat, F.; Hakim, A.A.; Dekany, I. Synthesis and utilization of poly (methylmethacrylate) nanocomposites based on modified montmorillonite. *Arabian J. Chem.* **2017**, *10*, 631–642. [[CrossRef](#)]
40. Mitchell, J.K.; Soga, K. *Fundamentals of Soil Behavior*; Wiley: Hoboken, NJ, USA, 2005.
41. Adeyemo, A.A.; Adeoye, I.O.; Bello, O.S. Adsorption of dyes using different types of clay: a review. *Appl. Water Sci.* **2017**, *7*, 543–568. [[CrossRef](#)]
42. Ferriol, M.; Gentilhomme, A.; Cochez, M.; Oget, N.; Mieloszynski, J. Thermal degradation of poly (methyl methacrylate)(PMMA): Modelling of DTG and TG curves. *Polym. Degrad. Stab.* **2003**, *79*, 271–281. [[CrossRef](#)]
43. Lee, Y.M.; Viswanath, D.S. Degradation of poly (methyl methacrylate)(PMMA) with aluminum nitride and alumina. *Polym. Eng. Sci.* **2000**, *40*, 2332–2341. [[CrossRef](#)]



© 2019 by the authors. Licensee MDPI, Basel, Switzerland. This article is an open access article distributed under the terms and conditions of the Creative Commons Attribution (CC BY) license (<http://creativecommons.org/licenses/by/4.0/>).